Supporting information for

Co-doped FeS_2 with Porous Structure for Efficient Electrocatalytic Overall Water Splitting

Lingfeng Gao †[a], Chengying Guo †[a], Xuejing Liu [a], Xiaojing Ma [a], Mingzhu Zhao [a], Xuan Kuang [a], Hua Yang [b], Xiaojiao Zhu [c], Xu Sun*[a], Qin Wei [a]

S1. Computational method and crystal structure

Computational method

All DFT calculations were carried out with projector-augmented wave method (PAW) [1] using the Vienna Ab initio Simulation Package (VASP). [2, 3] Perdew−Burke−Ernzerhof (PBE) exchange-correlation functional [4] with spin polarization was adopted to describe the electron-electron interaction. To take into account on-site coulomb repulsive interaction (PBE + U) [5], we employed the effective U value of 2 eV and 2.5 eV for respective localized Fe-*d* and Co-*d* orbitals.[6, 7] In all calculations, a plane-wave basis set with kinetic energy cutoff of 500 eV was used and the total energy was converged to less than 10^{-5} eV. The atomic positions were optimized until the force on each atom was less 0.02 eV/Å. As displayed in **Figure S1**, cubic pyrite (4 formula units per supercell) structure with space group $Pa\bar{3}$ and the cobalt doped FeS_2 compound $Co_xFe_{1-x}S_2$ ($x = 0.25$) were calculated with a 8 × 8 × 8 Monkhorst–Pack grid. [8] The optimized lattice parameters for the $Co_1Fe_3S_8$ (a' = 5.417 Å) and cubic pyrite (a = 5.404 Å) agree well with the experimental 5.417 Å. [9] Band structures were calculated along the highly symmetrical point in the Brillouin zone.

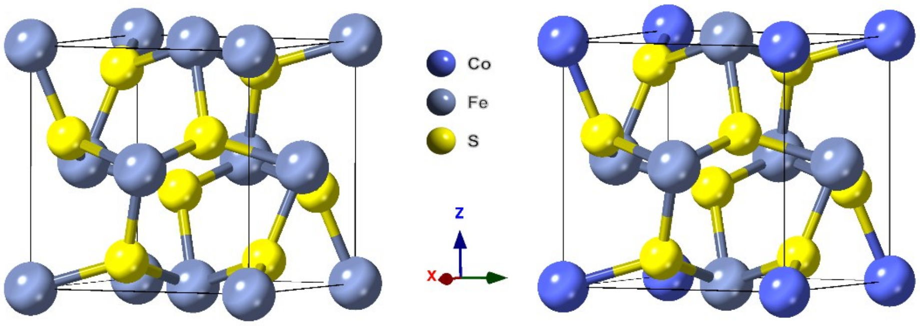

Figure S1. Crystal structures of pure FeS_2 (left) and the Co-doped FeS_2 (right). Royal blue, grey blue and yellow balls represent Co, Fe and S atoms, respectively.

To understand better the behavior of the cobalt doped FeS_2 compound with Co/Fe ratio of 1:3, we calculated the electronic band structure and density of states projected on the Fe and Co d-states and S p-states for both the $Co_xFe_{1-x}S_2$ ($x = 0.25$) and cubic FeS_2 in **Figure S1**. The results show that the optimized lattice parameter for the $Co_1Fe_3S_8$ (a' = 5.417 Å) is slightly larger than that for cubic FeS_2 (a = 5.404 Å) because of the larger Co atomic radius. The cubic FeS_2 is non-magnetic while the total magnetic moment of the $Co_1Fe_3S_8$ is $0.929\mu_B$ mainly resulting from the doped Co atom. Our computed band gap of cubic FeS_2 is about 0.87 eV, in agreement with other theoretical values.[10-13] The Fermi level is at the top of the valence band. However, The Fermi level for the $Co_1Fe_3S_8$ moves up and enter the conduction band. The peak electron state density in the valence band moves toward the lower energy and more delocalized. The cobalt doped FeS_2 compound is transformed from p type to n type semiconductor. Apparently, there are a number of conducting carriers that contributed by Co atoms near the bottom of the conduction band. To some extent the conductivity of the cobalt doped FeS_2 system is obviously improved.

S2. Electrochemical measurement and characterization

1. Electrochemical measurement

The electrochemical characterization was carried out on electrochemical station (CHI660B, China) using a classical three-electrode system in 1 M KOH solution with O_2-saturated. As-produced sample was used for the working electrode, graphite electrode as the counter electrode, Ag/AgCl electrode as the contrast electrode, respectively. The potential was calibrated against and converted to reversible hydrogen electrode (NHE). For the producing of working electrode, 5 mg of as-synthesized materials was dispersed in the 1 mL tailor-made solution of water/ethanol = 7/3. Then, 50 μL of superpolymer (Nafion solution, 5 wt%) was added to obtain a homogeneous emulsion with the help of sonication. 4 μL of the obtained solution was dropped on the clearly glassy carbon (GC) electrode. Specifically, the surface area of the GC was about 0.07 cm^2. 20 times of CV was carried out with the scan rate of 100 mV s^{-1} to stabilize the catalyst in the voltage range of 0.2 ~ -0.4 V (vs. NHE). Next, polarization curve was proceed by linear sweep voltammetry at a sweep rate of 5 mV s^{-1} in O_2 pre-saturated 1 M KOH. At the same time, the measurement of Ac impedance was recorded at the frequency range of 0.1 mHz to 100 kHz, take-off potential of -0.3 V (vs. NHE) and the amplitude of 5 mV. To confirm the excellent stability, the around-the-clock of cyclic voltammetry with a scan rate of 0.1 V s^{-1} was carried out for 1000 cycles between 0.2 V and -0.4 V (vs. NHE), after which LSV was performed at 5 mV s^{-1}. What's more, the number of active sites were received from the methods previous reported. [14, 15] The electrochemical measurement of OER was similarly with HER expect for the voltage range of 1.0 ~ 1.8 V (vs. NHE). Furthermore, the electrochemical measurement of overall water splitting via a two-electrode cell that $Co_{0.25}Fe_{0.75}S_2$/CC and other catalysts used as both anode and cathode at the same time.

2. Characterization

The surface morphologies structure of catalyst was surveyed with the equipment of Helios FIB SEM at 10.0 kV. Meanwhile, to explore the internal feature Transmission electron microscope (H-800 microscope, Hitachi, Japan) was carried out using an acceleration voltage of 200 kV. Furthermore, powder XRD pattern to analysis the crystalline structure was collected using Rigaku Smart Lab 9 kW. Spectral information was recorded in the extent of 10° ~ 70° 2θ with a step width of 0.01°/2θ. X-ray photoelectron spectra (XPS) were elucidated by ESCALAB 250 electron energy spectrometer (Thermo Fisher Scientific, USA) and Monochromated Al Kα 150 W was used to the X-ray excitation source. Finally, all the electrochemical measurement was recorded on electrochemical station (CHI660B).

S3. Calculation detailes

Potential vs. NHE calculation:

The measured potentials vs. Ag/AgCl were converted to the reversible hydrogen electrode (NHE) according to the following equation:

$E\ (\mathrm{NHE}) = E\ (\mathrm{Ag/AgCl}) + 0.197 + 0.059 \times \mathrm{pH}$

Active sites calculation:

Firstly, when measured the polarization curve, record the amount of electricity in the positive and negative directions at a sweep speed of 5 mV s^{-1}. The active sites is calculated by the following formula:

active sites (n) = $(Q_{+} + Q_{-}) / (F \times m)$

m represents the mass loading of electrocatalysts (~ 0.28 mg cm^{-2}), F is the Faraday constant (96487 C mol^{-1}).

S4. XRD spectrums of all catalysts

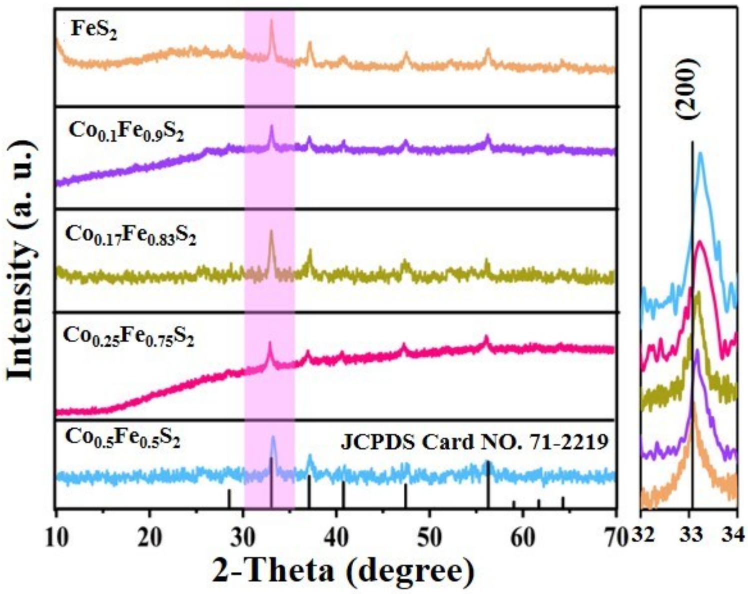

Figure S2. XRD spectra of all catalysts and the associated (200) plane of all catalysts.

S5. XPS survey of Co$_{0.25}$Fe$_{0.75}$S$_2$

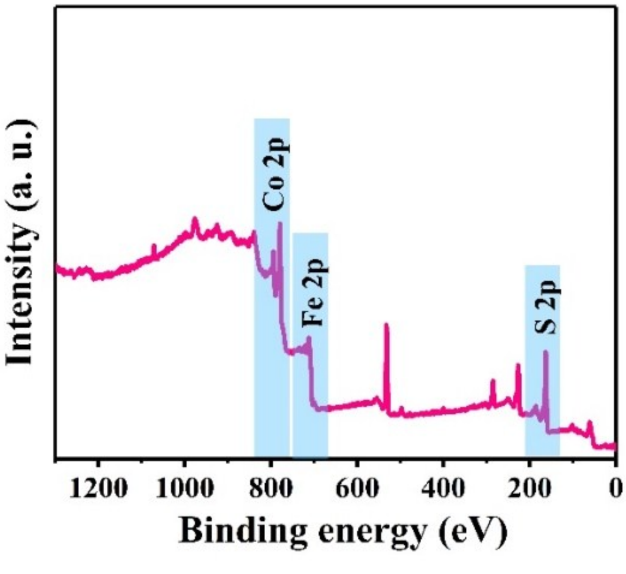

Figure S3. XPS survey of Co$_{0.25}$Fe$_{0.75}$S$_2$.

S6. SEM images of $Co_{0.5}Fe_{0.5}S_2$, $Co_{0.17}Fe_{0.83}S_2$ and $Co_{0.1}Fe_{0.9}S_2$

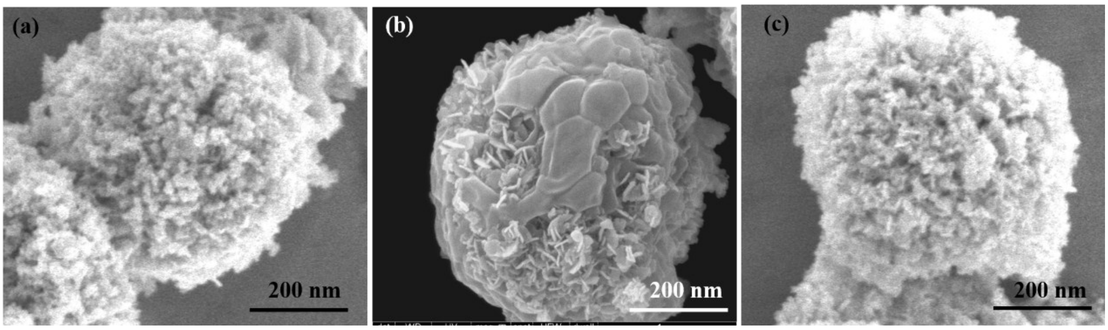

Figure S4. SEM images of (a) $Co_{0.5}Fe_{0.5}S_2$, (b) $Co_{0.17}Fe_{0.83}S_2$ and (c) $Co_{0.1}Fe_{0.9}S_2$.

S7. SEM images of FeS_2

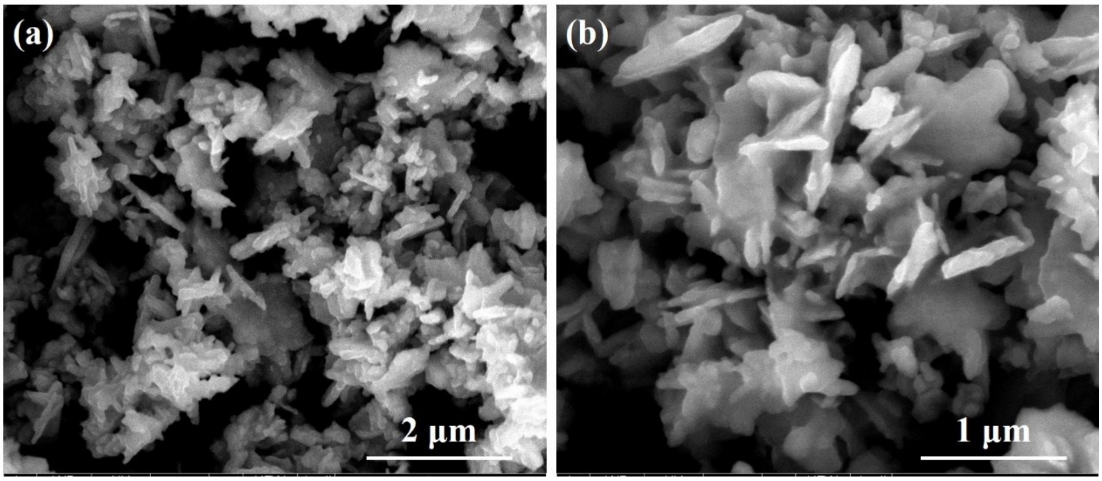

Figure. S5 SEM images of pure FeS_2.

S8. Surface area analysis

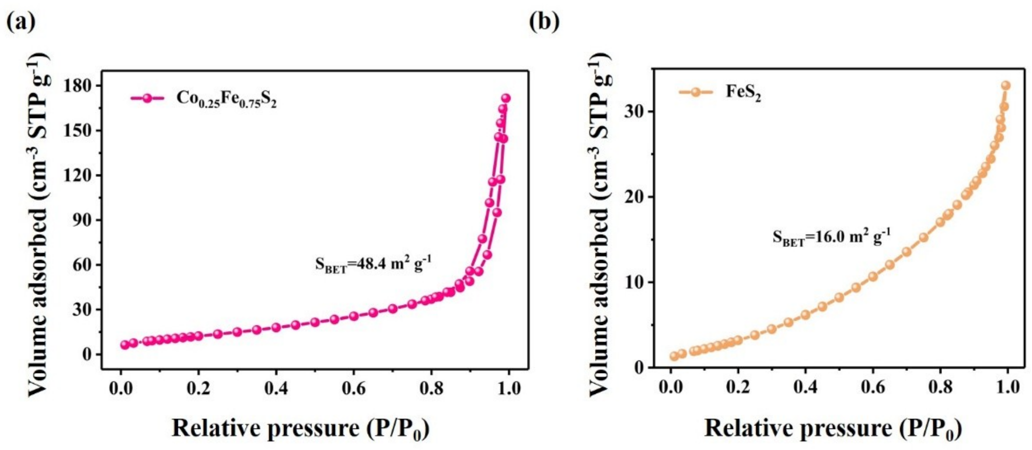

Figure S6. Nitrogen adsorption-desorption isotherms for (a) $Co_{0.25}Fe_{0.75}S_2$ and (b) FeS_2.

S9. EDS information of $Co_{0.25}Fe_{0.75}S_2$

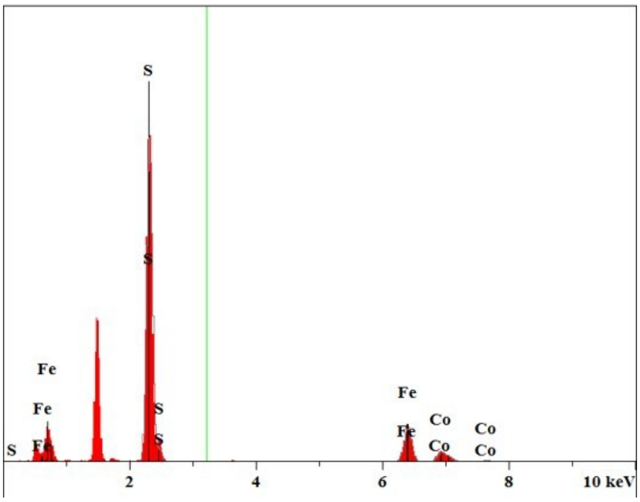

Figure S7. EDS spectrum of $Co_{0.25}Fe_{0.75}S_2$.

Elt.	Line	Intensity (c/s)	Conc.	Units	Error 2-sig	MDL 3-sig	
S	Ka	966.91	54.824	wt.%	0.658	0.211	

Fe	Ka	139.99	33.167	wt.%	1.081	0.533	
Co	Ka	39.85	12.008	wt.%	0.799	0.606	
			100.000	wt.%			Total

Table S1. Elemental components information of $Co_{0.25}Fe_{0.75}S_2$.

S10. Electrocatalytic activity comparison for HER

	Overpotential (mV) [a]	Tafel Slopes (mV dec^{-1})	C_{dl} (mF cm^{-2}) [b]	R_s (Ω) [c]	R_{ct} (Ω) [d]	Number of active sites ($\times10^{-3}$ mol g^{-1})
$Co_{0.5}Fe_{0.5}S_2$	290	81	7.0	14.9	62	4.1
$Co_{0.25}Fe_{0.75}S_2$	267	58	9.0	14.2	33	6.8
$Co_{0.17}Fe_{0.83}S_2$	280	65	8.8	13.6	38	6.3
$Co_{0.1}Fe_{0.9}S_2$	285	70	7.5	14.7	56	5.4
FeS_2	354	96	4.4	15.7	233	1.1

a: The overpotential value when current density is 10 mA cm^{-2} for HER in 1 M KOH solution.

b: The value of C_{dl} calculated at 0.05 V (vs. NHE) of CV.

c: Series resistances.

d: Charge transfer resistance at -0.3 V (vs. NHE).

Table S2. Electrocatalytic activity comparison of $Co_{0.5}Fe_{0.5}S_2$, $Co_{0.25}Fe_{0.75}S_2$, $Co_{0.17}Fe_{0.83}S_2$, $Co_{0.1}Fe_{0.9}S_2$ and FeS_2 for HER.

S11. Equivalent circuit for modeling the impedance results

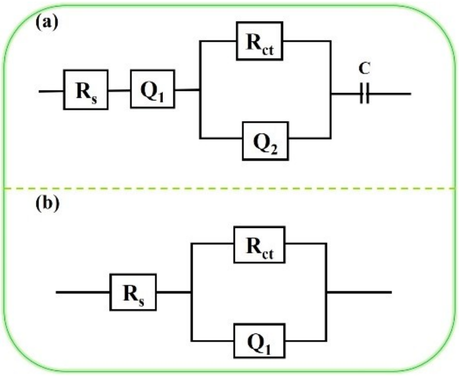

Figure S8. Equivalent circuit for modeling the impedance results. (a) The equivalent circuit of the catalysts with Co atoms. (b) The equivalent circuit of pure FeS_2.

S12. Cyclic voltammetry curves

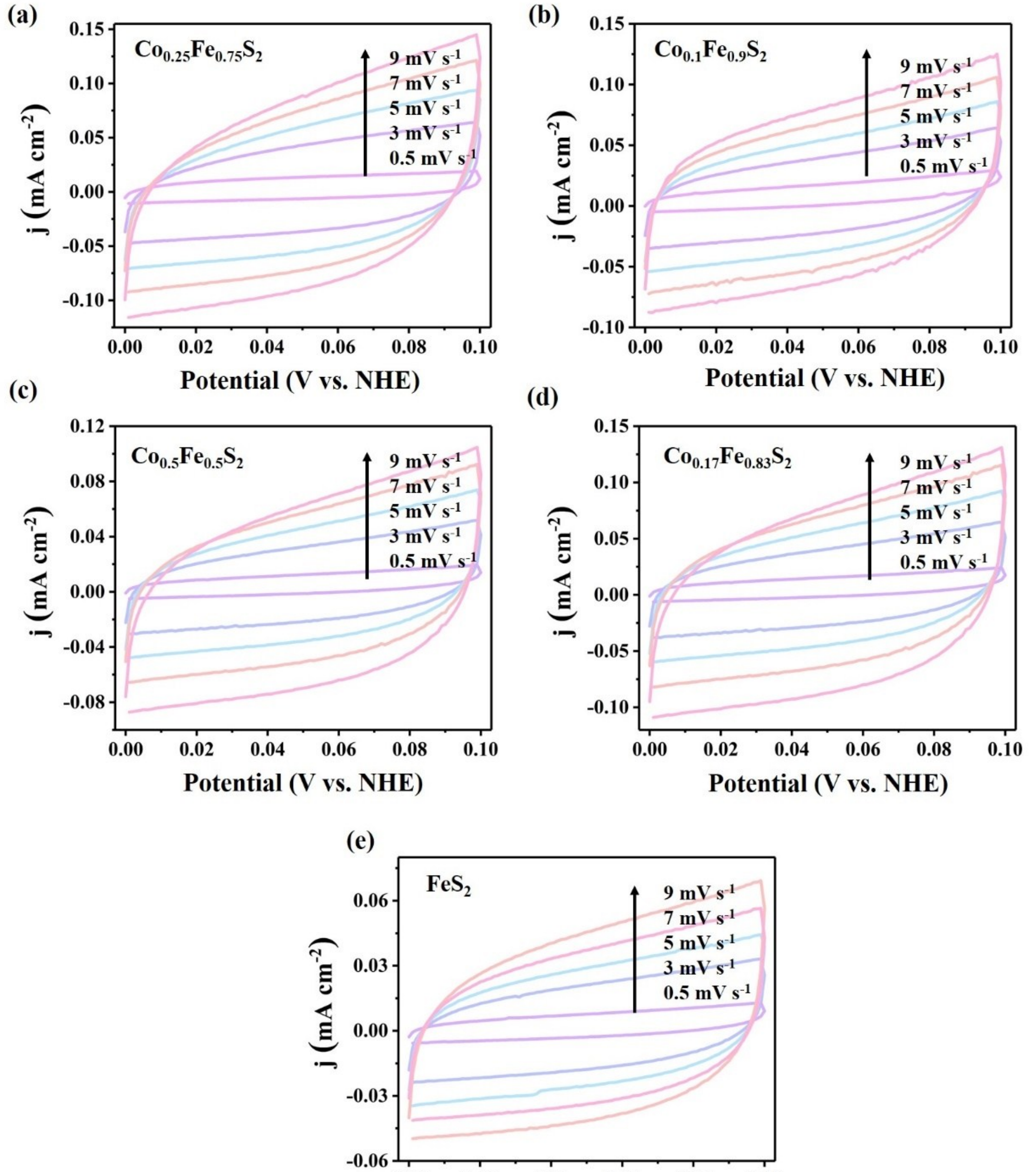

Figure S9. Cyclic voltammetry curves of (a) $Co_{0.25}Fe_{0.75}S_2$, (b) $Co_{0.1}Fe_{0.9}S_2$, (c) $Co_{0.5}Fe_{0.5}S_2$, (d) $Co_{0.17}Fe_{0.83}S_2$, (e) FeS_2.

S13. Current density normalized by the C_{dl} and BET surface area

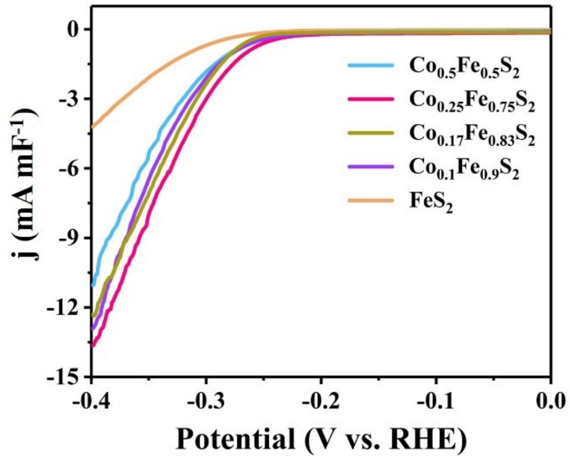

Figure S10. Polarization curves of $Co_{0.5}Fe_{0.5}S_2$, $Co_{0.25}Fe_{0.75}S_2$, $Co_{0.17}Fe_{0.83}S_2$, $Co_{0.1}Fe_{0.9}S_2$ and FeS_2 normalized by the C_{dl}.

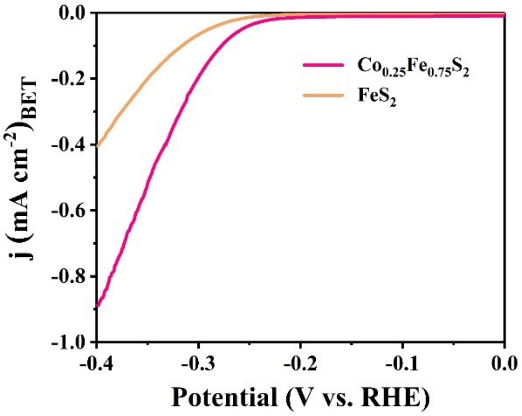

Figure S11. Polarization curves of $Co_{0.25}Fe_{0.75}S_2$ and FeS_2 normalized by the BET surface area.

S14. Mass activity of all catalysts

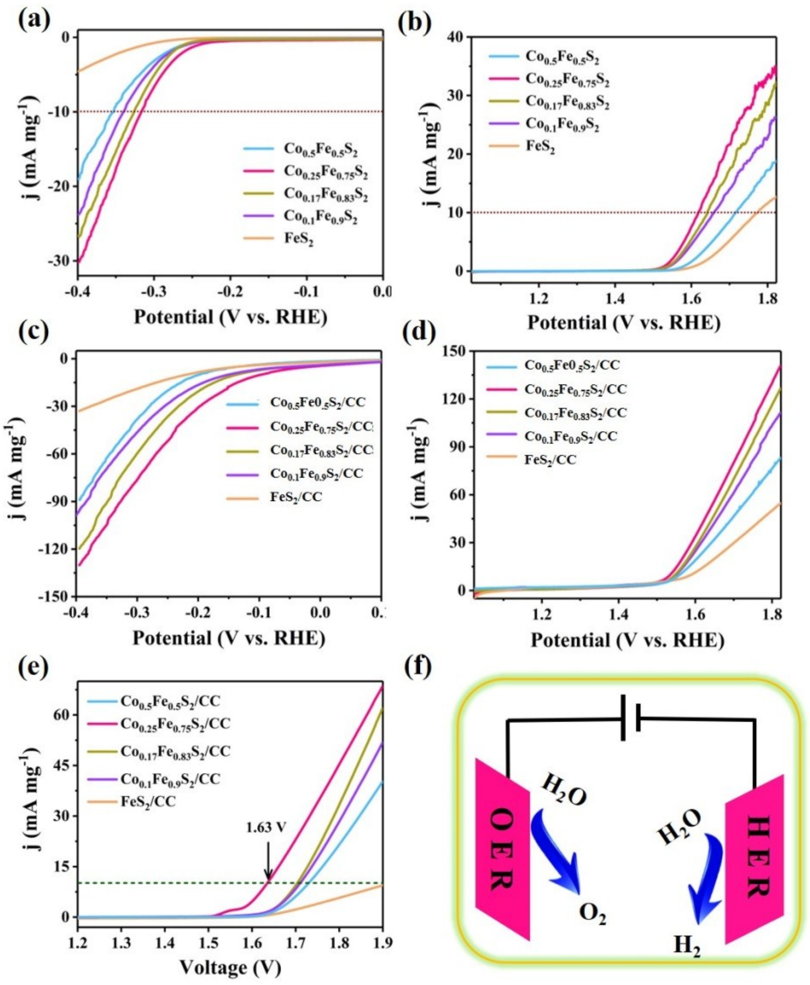

Figure S12. (a) Mass activity of all catalysts coated on a GC electrode for HER. (b) Mass activity of all catalysts coated on a GC electrode for OER. (c) Mass activity of all catalysts loading on a CC for HER and OER. (d) Mass activity of all catalysts loading on CC used as both anode and cathode for overall water splitting. (e) Schematic for full water splitting.

S15. XPS spectra of the catalyst before and after OER

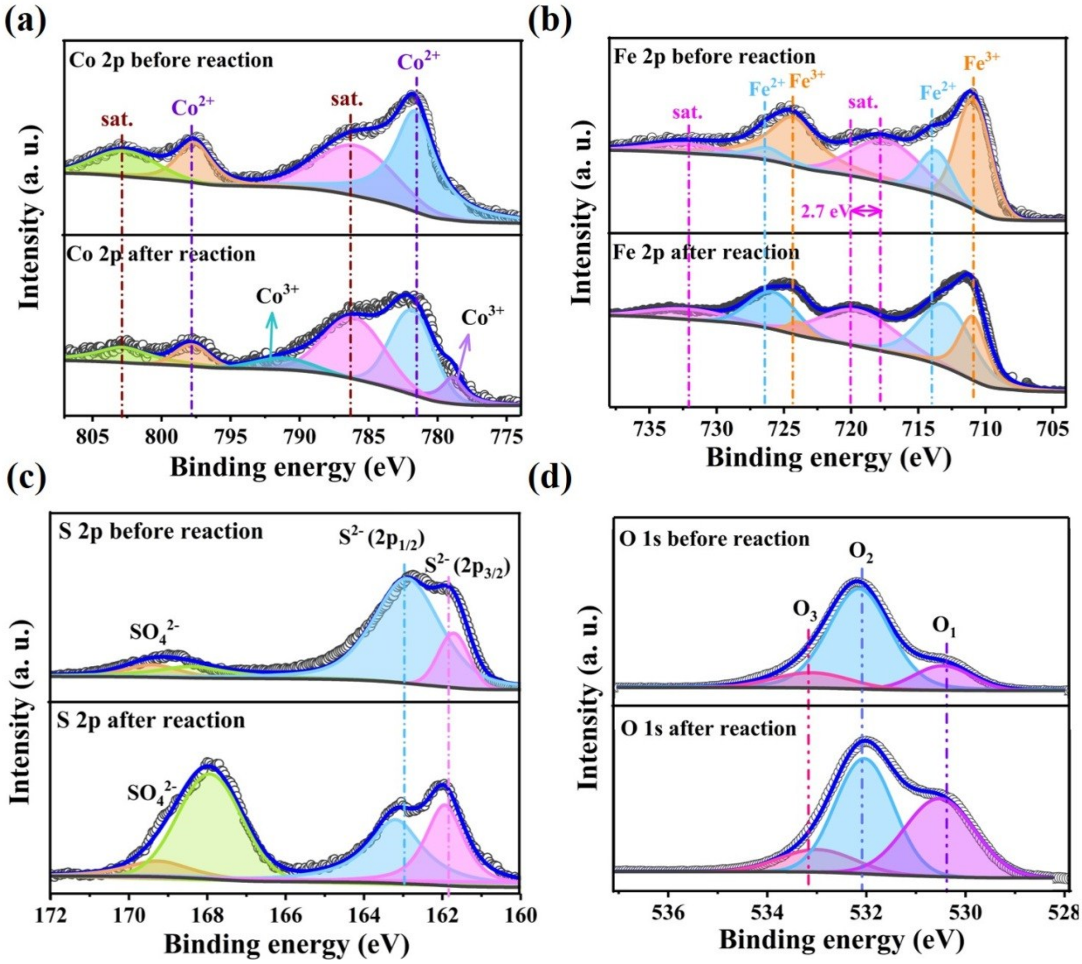

Figure S13. XPS spectra of $Co_{0.25}Fe_{0.75}S_2$ before and after OER. (a) Co 2p spectrm (b) Fe 2p spectrum (c) S 2p spectrum and (d) O 1s spectrum of $Co_{0.25}Fe_{0.75}S_2$ before and after OER.

S16. XPS survey of $Co_{0.25}Fe_{0.75}S_2$ after OER

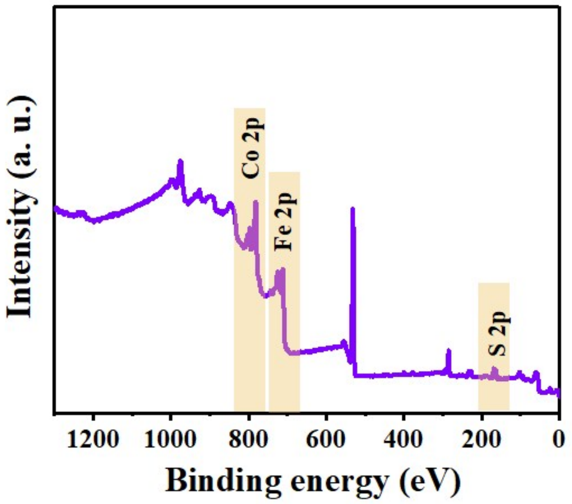

Figure S14. XPS survey of $Co_{0.25}Fe_{0.75}S_2$ after OER.

S16. LSV curve of $Co_{0.25}Fe_{0.75}S_2$ coated on a GC electrode for overall water splitting

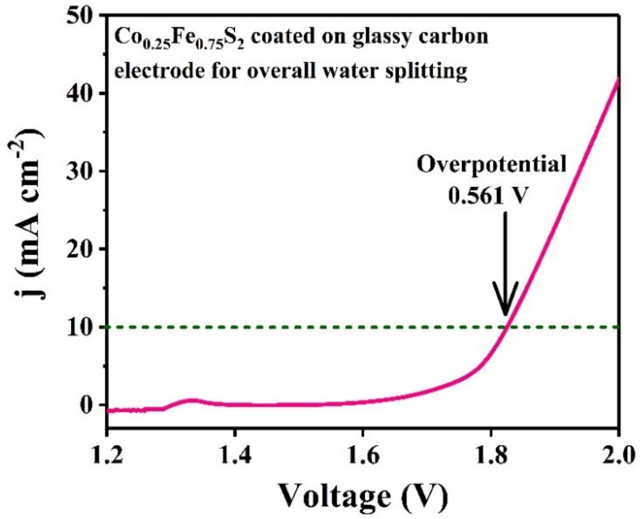

Figure S15. LSV curve of $Co_{0.25}Fe_{0.75}S_2$ coated on a GC electrode as both anode and cathode for overall water splitting.

S17. Electrocatalytic activity comparison for OER

	Overpotential (mV) [a]	Tafel Slopes (mV dec^{-1})
$Co_{0.5}Fe_{0.5}S_2$	385	69
$Co_{0.25}Fe_{0.75}S_2$	324	50
$Co_{0.17}Fe_{0.83}S_2$	337	57
$Co_{0.1}Fe_{0.9}S_2$	343	59
FeS_2	422	78

a: The overpotential value when current density is 10 mA cm^{-2} for OER in 1 M KOH solution.

Table S3. Electrocatalytic activity comparison of all catalysts for OER.

S18. Mass activity comparison of all catalysts

	η^a for HER (mV)	η^b for OER (mV)	η^c for HER (mV)	η^d for OER (mV)	η^e for water splitting (V)
$Co_{0.5}Fe_{0.5}S_2$	356	485	201	330	1.73
$Co_{0.25}Fe_{0.75}S_2$	310	381	100	304	1.63
$Co_{0.17}Fe_{0.83}S_2$	326	410	135	315	1.70
$Co_{0.1}Fe_{0.9}S_2$	340	432	152	322	1.71
FeS_2	---	541	221	362	1.90

a: The overpotential for HER to reach 10 mA mg^{-1} of the catalysts coated on aGC electrode.

b: The overpotential for OER to reach 10 mA mg^{-1} of the catalysts coated on a GC electrode.

c: The overpotential for HER to reach 10 mA mg^{-1} of the catalysts located on the carbon cloth (CC) with high conductivity.

d: The overpotential for OER to reach 10 mA mg^{-1} of the catalysts located on the CC with high conductivity.

e: The overpotential for overall water splitting to reach 10 mA mg^{-1} of the catalysts located on the CC with high conductivity.

Table S4. Mass activity comparison of all catalysts coated on GC electrode and located on CC for HER, OER and overall water splitting.

S19. Catalytic comparison to reported bifunctional catalysts

	η[a] for HER (mV)	η[b] for OER (mV)	η[c] for water splitting (V)
Co-FeS$_2$ This work	**71**	**282**	**1.60**
NiS/NiS$_2$ [16]	---	---	1.62
CoS$_2$–MoS$_2$ [17]	97	272	1.60
NiCo$_2$S$_4$ [18]	190	---	1.68
Co$_9$S$_8$/WS$_2$ [19]	138	---	1.65
Ni(OH)$_2$/Ni$_3$S$_2$ [20]	105	240	1.57
Zn$_{0.975}$Co$_{0.025}$S/CoS$_2$ [21]	152	270	1.59
Ni$_3$S$_2$/Co$_9$S$_8$ [22]	---	---	1.55

Table S5. Reported bifunctional catalysts based on transition metal sulfides for water splitting recently.

S20. Bifunctional catalysts loading on the support for water splitting

	η[a] for HER (mV)	η[b] for OER (mV)	η[c] for water splitting (V)
Co-FeS$_2$ This work	**267**	**324**	**1.60 (10 mA cm $^{-2}$)**
Fe-CoP/Ti [23]	---	---	1.6 (10 mA cm $^{-2}$)
CoO$_x$@CN /NF [24]	232	380	1.55 (20 mA cm $^{-2}$)
Co$_4$Ni$_1$P NTs/ Ni foam [25]	129	245	1.59 (10 mA cm $^{-2}$)

a: The overpotential for HER to reach 10 mA cm^{-2} of the catalysts coated on a GC electrode.

b: The overpotential for OER to reach 10 mA cm^{-2} of the catalysts coated on a GC electrode.

c: The overpotential of the catalysts located on the surpport with high conductivity.

Table S6. Reported bifunctional catalysts loading on the support for overall water splitting recently.

References

1 P. E. Blöchl, Phys. Rev. B: Condens. Matter Mater. Phys., 1994, **50**, 17953-17979.

2 G. Kresse and J. Furthmuller, Phys. Rev. B: Condens. Matter Mater. Phys., 1996, **54**, 11169-11186.

3 G. Kresse and J. Furthmuller, Comput. Mater. Sci., 1996, **6**, 15-50.

4 J. P. Perdew, K. Burke and M. Ernzerhof, Phys. Rev. Lett., 1996, **77**, 3865-3868.

5 V. I. Anisimov, F. Aryasetiawan and A. I. Lichtenstein, J. Phys.: Condens. Matter, 1997, **9**, 767-808.

6 N.Y. Dzade and N.H. de Leeuw, Phys. Chem. Chem. Phys., 2017, **19**, 27478-27488.

7 I. Khan and J. S. Hong, Nanotechnology, 2016, **27**, 385701.

8 H. J. Monkhorst and J. D. Pack, Phys. Rev. B, 1976, 1**3**, 5188-5192.

9 G. Brostigen and A. Kjekshus, Acta Chem. Scand., 1969, **23**, 2186-2188.

10 E. K. Li , K. H. Johnson, D. E. Eastman and J. L. Freeouf, Phys. Rev. Lett., 1974, **32**, 470-472.

11 A. Ennaoui, S. Fiechter, C. Pettenkofer, N. Alonso-Vante, K. Bker, M. Bronold, C. Hopfner and H. Tributsch, Sol. Energy Mater. Sol. Cells, 1993, **29**, 289-370.

12 L. Wu, N. Y. Dzade, L. Gao, D. O. Scanlon, Z. Öztürk, N. Hollingsworth, B. M. Weckhuysen, E. J. M. Hensen, N. H. de Leeuw and J. P. Hofmann, Adv. Mater., 2016, **28**, 9602-9607.

13 A. Krishnamoorthy, F. W. Herbert, S. Yip, K. J. Van Vliet, B. Yildiz, J. Phys.: Condens. Matter, 2012, **25**, 045004.

14 M. Gao, W. Sheng, Z. Zhuang, Q. Fang, S. Gu, J. Jiang and Y. Yan, J. Am. Chem. Soc., 2014, **136**, 7077-7084.

15 L. Wu, Q. Li, C. H. Wu, H. Zhu, A. Mendoza-Garcia, B. Shen, J. Guo and S. Sun, J. Am. Chem. Soc., 2015, **137**, 7071-7074.

16 Q. Li, D. Wang, C. Han, X. Ma, Q. Lu, Z. Xing and X. Yang, J. Mater. Chem. A, 2018, **6**, 8233-8237.

17 J. Hou, B. Zhang, Z. Li, S. Cao, Y. Sun, Y. Wu, Z. Gao and L. Sun, ACS Catal., 2018, **8**, 4612-4621.

18 A. Sivanantham, P. Ganesan and S. Shanmugam, Adv. Funct. Mater., 2016, **26**, 4661-4672.

19 S. Peng, L. Li, J. Zhang, T. L. Tan, T. Zhang, D. Ji, X. Han, F. Cheng and S. Ramakrishna, J. Mater. Chemi. A, 2017, **5**, 23361-23368.

20 X. Du, Z. Yang, Y. Li, Y. Gong and M. Zhao, J. Mater. Chem. A, 2018, **6**, 6938-6946.

21 Z. Yu, Y. Bai, S. Zhang, Y. Liu, N. Zhang and K. Sun, J. Mater. Chem. A, 2018, **6**, 10441-10446.

22 J. Lin, H. Wang, Y. Du, C. Zhao, J. Qi, J. Cao, W. Fei. J. Feng, J. Power Sources, 2018, **401**, 329-335.

23 C. Tang, R. Zhang, W. Lu, L. He, X. Jiang, A. Asiri, X. Sun, Adv Mater., 2017, **29**, 1602441-1602446.

24 H. Jin, J. Wang, D. Su, Z. Wei, Z. Pang, Y. Wang, J. Am. Chem. Soc. 2015, **137**, 2688−2694.

25 L. Yan, L. Cao, P. Dai, X. Gu, D. Liu, L. Li, Y. Wang, X. Zhao, Adv. Funct. Mater. 2017, **27**, 1703455-1703464.